Comparing the evolvability of an ancestrally reconstructed and modern adenylate kinase

MacKenzie Patterson[1,2]*, Hannes Ludewig[1-3]*, Christopher Wilson[2,5], Daniel R. Woldring[2,6], Chansik Kim[2,7], Aedan Using[2], Joseph Irvin[2,8], Douglas L. Theobald[4] & Dorothee Kern[1,2#]

[1]Department of Integrated Structural and Computational Biology, Scripps Research & Howard Hughes Medical Institute, La Jolla, CA, USA
[2]Department of Biochemistry & Howard Hughes Medical Institute, Brandeis University, Waltham, MA, USA
[3]Department of Biology & Howard Hughes Medical Institute, Brandeis University, Waltham, MA, USA
[4]Department of Biochemistry, Brandeis University, Waltham, MA, USA
[5]Current affiliation: Vividion Therapeutics, San Diego, CA, USA
[6]Current affiliation: Department of Chemical Engineering and Materials Science & Institute for Quantitative Health Science and Engineering, Michigan State University, East Lansing, MI, USA
[7]Current affiliation: DAAN Biotherapeutics, Seoul, 04323, Republic of Korea
[8]Current affiliation: Department of Biology, University of Rochester, Rochester, NY, USA

[#]To whom correspondence should be addressed: dkern@scripps.edu
*These authors contributed equally.

Abstract

Directed evolution revolutionized the field of protein engineering by establishing a highly customizable framework to produce enzymes with enhanced catalytic power for a wide range of functions. However, modern enzymes subjected to directed evolution frequently plateau in improvement due to entrapment in local maxima on their fitness landscapes. Ancestral enzymes have been proposed as superior starting points for directed evolution due to their increased thermostability. Here we propose and experimentally test an alternative foundation that is independent of ancestral thermostability. We posit that the enhanced evolvability of ancestrally reconstructed sequences is due to their inference from the surviving evolutionary trajectories that led to modern-day sequences. All other unsuccessful trajectories from less evolvable ancestors were lost by extinction. Using thermophilic ancestral and modern adenylate kinases with matching thermostability, we performed independent *in vivo* and *in vitro* single-round selection experiments for enzyme activity. In both settings, the ancestral enzyme tolerates a larger number of mutations, resulting in more viable and genetically diverse variants than its modern descendants. As mutational robustness drives evolvability, we demonstrate an intrinsic evolvability of reconstructed ancestral sequences that makes them superior starting points for directed evolution endeavors.

Introduction

Ancestral sequence reconstruction (ASR) has emerged as a fundamental approach in understanding the molecular principles of protein evolution[1]. This technique has been essential in illuminating central evolutionary questions spanning proton pumps[2], bacterial carbon fixation[3], evolution of allostery[4], and thermo-adaptation of enzymes[5]. Besides their role in fundamental research, ancestral proteins have accelerated protein engineering efforts in biomedicine and biotechnology[6], including the engineering of biosensors[7], terpene cyclases[8], and dehalogenases[9], among others[10,11]. This impact stems from

improved expression levels, often increased (thermo)stability, and substrate promiscuity rendering these ancestrally resurrected proteins into superior scaffolds for enzyme engineering efforts[12,13]. Importantly, these features are hallmarks of highly evolvable sequences[14], leading many to hypothesize that ancestral sequences are more evolvable relative to their modern counterparts[6,12,14–16].

Ancestors have indeed served as starting points for successful directed evolution (DE) campaigns and rational protein design endeavors[17–19]. Despite these advantages and hypotheses, direct experimental evidence comparing the evolvability of ancestral and extant proteins remains limited[17]. Understanding the molecular basis for enhanced evolvability is particularly important[20], as protein engineers routinely invest considerable effort to impart mutational robustness onto less evolvable starting points through approaches such as extensive library screening[21], neutral drift[22,23], chaperone overexpression[24], or computational stability enhancement[25,26].

Given that phenotypic robustness (a capacity to tolerate mutations) is a known driver of evolvability[27] and that thermostability enhances robustness[28], it has been generally assumed that the enhanced thermostability often found in ancestrally resurrected proteins underlies their increased evolvability[13,16,20,21,29–31]. If thermostability is the reason for better evolvability of ancestral proteins, one could simply use modern thermophilic proteins as starting points. Here we propose an alternative explanation: Ancestrally reconstructed sequences display higher evolvability because they are back-calculated based on only modern variants arising from evolutionary selection of the most evolvable sequences. The vast majority of sequences went extinct because of their lower robustness.

To test our hypothesis, we compared the evolvability of a thermophilic modern adenylate kinase (Adk) and its thermophilic ancestrally reconstructed counterpart[5] by assessing the clonal and mutational diversity that emerged after a single round of mutation and selection. We indeed observed that the ancestral enzyme tolerates a much larger number of viable variants, which also displays a higher degree of sequence diversity (mutations per gene) than the modern enzyme. Since both Adks are thermophilic, these results support our hypothesis that improved evolvability of ancestrally reconstructed sequences is an inherent property that stems from the evolutionary selection uncovered by ASR rather than thermostability.

Results

A weak-link selection platform couples adenylate kinase activity to *E. coli* fitness

We reasoned that, if ancestral Adks were more evolvable than their modern counterparts, an ancestral Adk would, due to mutational robustness, tolerate a greater depth of clonal and sequence diversity, effectively resulting in a larger number of viable variants (Fig. 1A). Since *adk* is an essential gene and its activity has been shown to correlate with organismal fitness[32,33], we used *adk* as a “weak link”[32] for organismal fitness of *E. coli* strains expressing primordial and modern *adk*s and used their doubling times as a proxy for Adk activity. To accomplish this, we employed a λ red recombination and complementation placeholder plasmid (pKOCOMP-*adk*)[34] to knock out genomic Ec*adk*

and rescue Adk activity in *Escherichia coli* BW25113 with thermophilic Adks: namely ancestor 1 (ANC1) and Adk from *Caldanaerobacter subterraneus* (CsAdk), respectively (first step in scheme shown in Supplementary Fig. 1). Doubling time measurements between 10 ºC and 35 ºC showed that below 25 ºC, both strains complemented with ANC1 or CsAdk on the placeholder plasmid grew more slowly than their parent *E. coli* strain (Fig. 1B). This slower growth rate parallels their decreased k_{cat} values at these temperatures when compared to EcAdk (Fig. 1B), highlighting that Adk activity determines cellular fitness between 10 ºC and 20 ºC. Seeking to verify that this fitness loss originated from lower Adk activity and not from the process of genetic manipulation, we repeated the doubling time measurement of an *adk* knockout *E. coli* strain harboring Ec*adk* on the plasmid. Indeed, the recorded doubling time was within error of WT *E. coli*. Notably, at 25 ºC and above, no significant difference in growth rate is observed, implying that the speed of Adk (EcAdk: $k_{cat,40\,°C}$: 673.4 s^{-1}, CsAdk: $k_{cat,40\,°C}$: 80.2 s^{-1}, ANC1: $k_{cat,40\,°C}$: 189.1 s^{-1}) is no longer the bottleneck (weak link) for growth at these temperatures.

Emboldened by these results, we set out to produce an "acceptor strain" (AS) which could be readily transformed with high efficiency, thus being easily rescued by any sufficiently active *adk* (either a WT plasmid or a plasmid library of *adk* mutants) in a directed evolution experiment. We produced this AS using the previously created Ec*adk* KO strain (BW25113 *adk*::Cm [pKOCOMP-Cs*adk*]) which was further transformed with the ancillary plasmid (pI-SceI). Since the placeholder plasmid we had used for genomic Ec*adk* knockout encodes CsAdk, the AS can survive on CsAdk activity, until the strain is further transformed by the desired *adk*. The placeholder could then be removed from the resulting strain by rapid and conditional self-depletion to ensure that cell survival is solely dependent on the *adk* of interest, thereby avoiding an advantage of insufficiently active *adks*[34]. This comprehensive self-depletion is facilitated by two indispensable features of the placeholder: a heat-sensitive origin of replication, enabling plasmid curing at 42 ºC, and a recognition site for the inducible restriction endonuclease, I-*Sce*I, which is encoded on an auxiliary plasmid pI-SceI (Supplementary Fig. 1 and Supplementary Table 1). To verify this method, we first transformed the AS with plasmids holding the ancestral or modern *adks* and confirmed that the doubling times of these "knock-in" strains were strongly correlated with their corresponding k_{cat} at 20 ºC (Pearson r = -0.87; Fig. 1C).

Most importantly, this strain engineering allowed selection experiments using libraries of ancestral and modern Adks. We transformed the AS with libraries of either ANC2 or one of two modern Adks, *Bacillus subtilis* (BsAdk) and *Geobacillus stearothermophilus* (GsAdk), then grew the cells at 18 ºC after confirming successful removal of the placeholder plasmid. The expectation is that (i) only cells expressing active Adk variants can grow and (ii) higher-activity Adk variants will outcompete slower ones and enrich in the culture. Sanger sequencing colonies of the selected ANC2 library indeed showed the greatest population diversity at both 42 ºC and 18 ºC compared to the modern Adks (Supplementary Fig. 2), indicative of the ancestral sequence being more robust. However, these first experiments had two limitations. 1) Comparisons were convoluted by differences in k_{cat} and thermostability (T_m) among parental Adks: GsAdk is thermophilic but ~8x slower at low temperatures than ANC2, while BsAdk is mesophilic and ~3x slower than ANC2 (Fig. 1D). These discrepancies likely influenced the relative response to

selective pressures during the necessary 42 ºC placeholder curing and at 18 ºC selection for BsAdk and GsAdk library strains. 2) Sanger sequencing limited the depth (number of variants) that we could identify, thereby impeding highly quantitative comparisons of population diversity. Below we describe how we overcame these two limitations.

We endeavored to find the most similar ancestor/extant pair with respect to k_{cat} and T_m values. After extensive search, we identified Adk from *Anoxybacillus flavithermus* (AfAdk) as the best match to ANC2 with only a 1.8-fold lower k_{cat} and a 9 ºC lower T_m (Fig. 1D). Sequence differences between the two Adks (72.4% sequence identity) are globally distributed (Fig. 1E and Supplementary Fig. 3). Notwithstanding those small differences in k_{cat} and T_m, the ANC2 and AfAdk WT knock-ins unveil similar fitness at 20 ºC, as demonstrated by their doubling times, which are much greater (slower growth) than those exhibited at 37 ºC and 42 ºC where Adk activity is no longer rate-limiting for *E. coli* growth (Fig. 1F). To confirm that both enzymes are poorly adapted to 20 ºC, we used a discontinuous high-pressure liquid chromatography (HPLC) assay to measure the temperature dependence of ANC2 and AfAdk k_{cat} values between 10 ºC and 90 ºC. We found they have maximal activities at 70 ºC and 60 ºC, respectively, with ANC2 having a much steeper increase in activity with temperature which is in agreement with other ancestral Adks[5], but importantly show similar activities at low temperatures (Fig. 1G).

Long-term survival selection demonstrates enhanced evolvability of ancestral over modern adenylate kinase

Aiming to assess Adk evolvability more quantitatively, we returned to selection experiments utilizing error-prone PCR libraries of our newly identified pair, ANC2 and AfAdk. In addition to baffled culture flasks, we grew both libraries in a turbidostat[35], which served as a suitable, automated alternative allowing for temperature regulation with continuous recording and control of optical density at 650 nm (Fig. 2A). Second, we employed nanopore sequencing adapted from Karst *et al.*[36], to quantitatively compare population composition of flasks against turbidostat cultures with much higher sequencing depth than Sanger sequencing (Supplementary Fig. 4 and Supplementary Table 1-3). We found no differences in the survivable sequences identified from selection experiments done in flasks versus in the turbidostat (Supplementary Fig. 5). We next performed long-term selection experiments in the turbidostat, where we could continuously record doubling times, quantify population diversity via next-generation sequencing, and assess enzymatic activities of enriched individual Adks (Fig. 2A).

To ensure that selection experiment outcomes were not impacted by library diversity, we sequenced ANC2 and AfAdk libraries and quantified their diversity to be on the order of 10^4 unique sequences. Notably, AfAdk library was slightly more diverse than the ANC2 library (Supplementary Fig. 6). After 8 days of selection AS-ANC2lib exhibited higher fitness than AS-AfAdklib as judged by doubling times of 180 and 230 min, respectively (Fig. 2B and Supplementary Fig. 7A; Kolmogorov-Smirnov $p = 1.9 \times 10^{-31}$). Characterization of population diversity implicated ANC2 as more robust, revealed by a broader distribution of the number of mutations per *adk* gene at all timepoints and temperatures (Fig. 2C). Further analysis of the nanopore sequencing revealed that not only did ANC2 tolerate more mutations per gene than AfAdk, but more importantly AS-

ANC2lib displayed a larger number of viable Adks than AS-AfAdklib during all timepoints (Fig. 2D-E and Supplementary Fig. 7B-D). The degree of enrichment of highly abundant Adks mirrors the trajectories of doubling time stabilization by each library strain. The most substantial changes in variant abundances occurred during an initial ~2-day growth adaptation, followed by a slow stabilization during the remainder of selection (Fig. 2B, D, E and Supplementary Fig. 7). Strikingly, after 8 days of selection, AS-ANC2lib contained 813 variants, 807 of which still accounted for ~23% of the population (Fig. 2D and Supplementary Fig. 7B). In stark contrast, AS-AfAdk population was composed of 293 different variants but dominated by the single mutant AfAdk-V4M (~80%, Fig. 2E and Supplementary Fig. 7C), despite starting from a 10^4 variant library that was even slightly larger than for ANC2. Not only was AfAdk-V4M the dominant winner of the AfAdk library selection at 20 ºC, but it also served as a compensatory mutation for almost all other low-abundance AfAdk variants in that selection (Fig. 2F). The large discrepancy in population diversities of ancestral and extant library strains was reproducible between biological replicates (Supplementary Fig. 8).

Catalytic activities of purified variants correlate with enrichment during selection

Overall, we observed that mutations in ANC2 were distributed globally throughout the Adk structure. Contrarily, position V4 acts as a hotspot in modern Adks based on its reproducible augmentation in modern library strains (Fig. 3A and Supplementary Fig. 2, 5, and 7). While the sequencing results convincingly exhibited greater robustness of ANC2 over AfAdk, we asked whether this trend extended to activity as well. To answer this, we used a colorimetric coupled assay to measure the ADK-catalyzed conversion from ADP to ATP and AMP of enriched ANC2 and AfAdk variants and determined that AfAdk-V4M displayed a 1.3-fold increased k_{cat} over WT AfAdk. This small increase in activity translates into a minute 0.28 kcal/mol difference in activation free energy, which is challenging to rationalize structurally. A plausible hypothesis is a difference in hinge dynamics affecting lid opening[37], which has been demonstrated to be the rate-limiting step[38]. These differences could be the result of alternative hinge 4 packing. In AfAdk-V4M, residue L72 (part of hinge 4) is now part of the second shell of the mutated residue 4, which resembles the arrangement in the faster ANC2 (judged by AlphaFold 3 prediction; Supplementary Fig. 9). Catalytic improvements within the AS-ANC2lib were more modest, with E166V exhibiting the greatest activity improvement of 1.1-fold over WT ANC2 (Fig. 3B, Supplementary Table 4). Despite these slight improvements, the enrichment of each highly abundant ANC2 variant was strongly correlated with its k_{cat} at 20 ºC (Pearson r = 0.87), confirming our prediction that *E. coli* expressing faster Adks would outcompete bacteria encoding for slower Adks (Fig. 3C).

Regulatory mutations reveal expression-mediated fitness effects during *in vivo* selection

Interestingly, we discovered that inadvertent mutations (unpreventably introduced during epPCR library preparation) in the 5′ untranslated region (5′ UTR) were selected for in ANC2 WT clones during library selection, with a deletion of cytosine 9 in the ribosomal binding site being most abundant ($RBS^{\Delta C9}$; Fig. 3D and Supplementary Fig. 10A, B, and H). Closer inspection of the other highly abundant ANC2 sequences revealed that all but one (ANC2-I4N:M6I) contained other enriched 5′ UTR mutations (Fig. 3E and

Supplementary Fig. 10C-H). Two of those enriched mutants (E166V and E23Q:K79I) contained the same RBS$^{\Delta C9}$ mutation selected for in WT (Fig. 3E and Supplementary Fig. 10E-F and H). This enrichment could possibly be caused by an elevated in-cell Adk concentration, leading to an increase in cellular Adk activity. Indeed, when we tested in-cell Adk concentration, we found that an ANC2 strain harboring a mutant RBS$^{\Delta C9}$ in its 5` UTR displayed a higher in-cell ANC2 concentration than its WT strain and consequently effectuated a faster doubling time (Fig. 3F-G). These results agree with previous work showing that selective pressure can act on enzyme concentration rather than function to ensure survival[39–41]. While we note that AS-AfAdklib WT also possessed two off-target mutations in the promoter, we found that it was outcompeted by V4M, which did not contain any off-target mutations (Supplementary Fig. 11).

To further rationalize the apparent accumulation of high-abundance variants, we measured k_{cat} values of low-abundance sequences that were viable but were not enriched above 2% during selection. On average, these lowly populated Adks had k_{cat} values that were similar to or lower than WT, with one exception in ancestral (ANC2-G104R: 1.2x WT activity) and extant (AfAdk-V4M:N142D: 1.2x WT activity) libraries. Furthermore, there was no detectable relationship between their k_{cat} values and their abundance after 8 days of selection (Supplementary Fig. 12). Most of these variants did not contain off-target mutations. We discovered a further complication in the interpretation of the *in vivo* selection, a high degree of plasmid multimerization in biological samples (Supplementary Fig. 13). Multimerized plasmids encoded multiple origins of replication, which may allow for increased Adk expression. Alternatively, recombination of inactive Adks with active ones on the same plasmid would convolute population diversity.

Orthogonal *in vitro* selection corroborates increased evolvability of reconstructed ancestral adenylate kinase

Despite these additional effects we found in our *in vivo* selection experiments (that are inherent to such experiments), the data robustly reveal that the ancestral enzyme is more evolvable than its modern counterpart. Nevertheless, to further buttress this key result, we sought to employ an orthogonal approach and turned towards traditional *in vitro* DE. To screen Adk variant activity, we used the coupled assay on lysates of *E. coli* BL21 (DE3) overexpressing epPCR variants of ANC2 or AfAdk (library diversity: 10^4 and Supplementary Fig. 14). To test that the coupled assay (which measures production of ATP) accurately measured ATP production by Adk, we used the addition of the Adk inhibitor AP5A as baseline and compared the ATP production of this inhibited lysate to lysate with added Mg^{2+}•ADP.

The distributions of lysate Adk velocities for BL21-ANC2lib and BL21-AfAdklib (Fig. 4A) were significantly different (Kolmogorov-Smirnov p = 7.79 x 10^{-6}), with BL21-ANC2lib generally exhibiting higher activities than BL21-AfAdklib (Kolmogorov-Smirnov p = 3.90 x 10^{-6}). While the mean velocities of these two distributions are similar (BL21-ANC2lib$_{mean}$ = 0.48, BL21-AfAdklib$_{mean}$ = 0.42), their medians are strikingly different (BL21-ANC2lib$_{median}$ = 0.34, BL21-AfAdklib$_{median}$ = 0.13), reflective of this shift of BL21-ANC2lib toward higher activity. As a testament to higher ANC2 robustness, we not only

observed fewer inactive BL21-ANC2lib Adks, but importantly also observed a higher number of variants with increased activity when compared to BL21-AfAdklib. Furthermore, BL21-AfAdklib variants exhibited a higher fraction with inactive and near-WT activities than BL21-ANC2lib.

These starkly different features of ancestral and modern activity profiles mirrored our *in vivo* findings and are in full agreement with our initial hypothesis that ancestral Adks would be more evolvable. We consequently expressed and purified variants with the highest lysate velocities (~1.5-fold improved over WT) to measure k_{cat} values (Fig. 4B, and Supplementary Tables 5, 6). Intriguingly, we discovered another highly favored mutation site for AfAdk: residue V204, found as single mutation and in combination with other mutations (Fig. 4C and Supplementary Fig. 15A). Similarly to our *in vivo* selection experiments we found that ancestral variants harbored more mutations per gene than extant ones (Fig. 4C, D and Supplementary Fig. 15A). Overall, we observed very little perturbation in T_m values of ANC2 and AfAdk variants but did notice that several ANC2 variants displayed slightly improved thermostabilities up to 3 ºC greater than WT in contrast to only one AfAdk variant with a 1 ºC increase in T_m (Fig. 4E). Taken together, these results suggest that ANC2 is more robust to varying amino acid changes than AfAdk.

Similarly to our *in vivo* selection, we could not find evidence that the superior robustness of ANC2 was accompanied by major catalytic improvements. There was a significant correlation between k_{cat} and lysate velocity for both libraries (Pearson $r_{ANC2} = 0.45$, $p_{ANC2} = 0.02$; Pearson $r_{AfAdk} = 0.73$, $p_{AfAdk} = 5.46 \times 10^{-4}$), confirming that lysate activity generally reports on k_{cat} (Supplementary Fig. 15B). The weaker correlation for ANC2 variants could be rationalized by determining Adk concentrations in screened cell lysates (using their k_{cat} values) and correlating these with the respective lysate velocities (Supplementary Fig. 15C). This revealed a moderate, but significant, correlation between lysate velocity and Adk concentration for ANC2 variants (Pearson $r_{ANC2} = 0.55$, $p_{ANC2} = 0.002$), but not for AfAdk variants (Pearson $r_{AfAdk} = 0.39$, $p_{AfAdk} = 0.11$). This suggests that mutations in ANC2 increased lysate activity in several cases by increasing cellular concentrations of folded Adk. This interpretation was further supported by comparing cellular Adk concentrations of ANC2 and AfAdk variants (Fig. 4F) which revealed a significant difference in their distributions (Kolmogorov-Smirnov $p = 0.025$), with the ancestral distribution shifted higher cellular Adk concentration than the modern distribution (Kolmogorov-Smirnov $p = 0.013$). This finding is unsurprising, since our applied selective pressure acts on total cellular Adk activity, which is the product of the enzymatic rate and total active enzyme concentration in the cell. Not only does this align with our *in vivo* selection experiments but is also in agreement with studies from Shamoo and others that have demonstrated that enzyme concentration is an easily tunable parameter when adapting to selective pressures on energy metabolism[32,33,41,42].

Discussion

Enzymes are remarkably facile catalysts promising ever-adapting solutions to emerging fields of technology, such as synthetic biology and biocatalysis. Key to unlocking these potentials are successful DE campaigns[43]. However, often DE is plagued by premature

optimization plateaus[16]. Thermostability can drastically enhance the evolvability of folded proteins by providing an elevated degree of mutational robustness to the evolving protein[28]. Specifically, this is caused by an increased tolerance towards neutral, yet destabilizing mutations, limiting the detrimental unfolding of the mutated scaffold, thus aiding the evasion of local fitness maxima, which can entrap evolutionary trajectories[16,27,44–47]. In consequence, such neutral networks open a larger and more diverse set of trajectories to traverse the fitness landscape more freely[27]. It has been proposed that such thermostability-driven robustness underpins the evolvability of ancestrally reconstructed sequences observed in many successful DE efforts[13,16,20,21,29–31]. If that were true, one could simply use thermostable modern sequences, which are more easily accessible than ancestors, as the best DE starting points.

Moreover, the proposed causal link between ancestral thermostability and robustness lacks conclusive experimental evidence. Alcalde *et al.* commented on this question when they sought to evolve type II RuBisCOs toward higher thermostability, starting from ancestrally reconstructed and bacterial (modern) starting sequences[17]. They concluded that ancestral RuBisCO (MRPro) was more tolerant towards mutations than the modern enzyme RubRr from *Rhodospirillum rubrum*, since a larger number of ancestrally derived clones were active in their high-throughput lysate screen. It is worth noting, however, that the data concerning populations and sequence diversity of ancestral and extant starting libraries were not comprehensively reported. On the other hand, Dickinson *et al.* used a phage-assisted continuous evolution (PACE) platform to probe the evolution of substrate specificity in the B-cell lymphoma-2 protein family, using extant and ancestral starting points, yet reported no observable difference in sequence diversity or evolvability. However, it is unclear if their Illumina (fragment-based) sequencing approach could deconvolute potential differences in clonal population diversity[46].

Given these conflicting results, we sought to systematically address this question: Is thermostability the driver of elevated evolvability found in ancestrally reconstructed sequences? Across two independent *in vivo* and *in vitro* evolution experiments initiated from thermophilic ancestral and modern Adks, we consistently observed greater population and sequence diversity for the ancestral Adk. This elevated mutational robustness is clearly uncoupled from ancestral thermostability. Furthermore, we observed increased ancestral robustness at 42 ºC (Fig. 2D-E), a temperature where Adk activity is no longer growth rate-limiting (Fig. 1B and F). This accentuates the effect this ancestral robustness has on the outcome of laboratory evolution.

Additionally, our ancestral variants selected for *in vitro* exhibited unchanged or even improved thermostability (Fig. 4E). This is generally advantageous for long term evolution (i.e. further rounds of DE), since it allows for accumulation of cryptic mutations. Such mutations invite epistasis, a highly desirable feature, especially when addressing particularly challenging enzyme engineering problems[30,45,47–49].

Our work speaks to a central question in the field of protein evolution, whether ancestral thermostability and robustness are a bias of ASR stemming from evolutionary model violation and erroneous introduction of consensus mutations[31,50–52] or rather an accurate

reflection of ancient environmental factors[5,53,54]. Given this ongoing debate and our results presented here which uncouple ancestral mutational robustness from thermostability, we propose an alternative framework on evolutionary survivorship: Since modern sequences used for ancestral reconstruction are by definition descendants of surviving sequences, accurate ASR is more likely to infer highly evolvable ancestral sequences. After all, their lineage persisted over evolutionary time, while less fit sequences went extinct. Critically, this does not imply that all ancestral sequences present billions of years ago were highly evolvable, but rather that the lineages we reconstruct by ASR had sufficient evolvability to adapt and survive. Thus, ASR reconstructs the highly evolvable "needle in the haystack" of historically explored sequence space, taking advantage of billions of years of selection. Therefore, the reconstructed sequence with the highest posterior probability was likely not the most probable back in time, but a highly evolvable one.

We acknowledge that our exploratory attempts to understand the phenomenon of ancestral evolvability fall short of gaining mechanistic insights into the biophysical and molecular underpinnings. For that, larger improvements in catalytic rates by many rounds of DE would be necessary, which was not the goal of this work. However, this study can provide a suitable starting point for such mechanistic endeavors, which should further aid the engineering of highly specific and powerful biomolecules.

Our findings and proposed framework highlight the unique place ancestrally reconstructed sequences occupy within the toolkit of DE methodology. Their computational accessibility combined with their enhanced evolvability, which allows for a more thorough exploration of sequence space, make these sequences more promising and economical DE starting points than extant sequences. Furthermore, using ASR as a first-choice approach does not sacrifice the opportunity to employ additional DE strategies, should the posed protein engineering problem prove challenging.

Methods

Data visualization and analysis

Data visualization and statistical analysis were performed using Python (https://www.python.org). Data manipulation and analysis were performed using Pandas, NumPy, and SciPy[55–57]. Matplotlib was used for data visualization[58]. AlphaFold 3 was used to predict the ligand-bound (2ADP, Mg^{2+}, Zn^{2+}) structures of Adks[59]. Crystal structures and AlphaFold 3 models of Adks were visualized with ChimeraX[60].

Construction of error-prone PCR libraries

Error-prone PCR libraries were prepared using the GeneMorph II EZ-Clone Domain Mutagenesis kit (Agilent) following modified manufacturer's instructions, unless stated otherwise. DpnI digest of the EZClone reaction was performed for 2 h at 37 ºC, followed by 16 h at 25 ºC, and was stored at 4-10 ºC until transformation (~4-8 h). To achieve a high mutation rate, 1 ng of plasmid (~ 0.15 ng of target) was amplified (35 cycles) using *adk*-flanking primers (Supplementary Table 1). XL10-Gold Ultracompetent *E. coli* cells (Agilent) were transformed with DpnI-treated library according to the manufacturer's

417 instructions. 50 µl of the recovered culture were plated on LB agar (50 µg/mL kanamycin
418 or 100 µg/mL ampicillin for *in vivo* and *in vitro* libraries, respectively). The remaining
419 volume was used to inoculate a 50 mL culture of LB (respective antibiotics) and was
420 grown overnight at 37 ºC in a shaking incubator (Infors HT Multitron AJ125) at 220 rpm.
421 Libraries were miniprepped (Qiagen) in 10X volume. DNA from 10-20 clones was Sanger
422 sequenced (Azenta) to estimate mutation rate and confirm correct annealing to the parent
423 plasmid. Libraries were stored at -20 ºC.
424
425 **Construction of adk knockout strains**
426 All knockout strains were made in *E. coli* (BW25113) using an adapted protocol from
427 Billerbeck & Panke (Supplementary. S1)[34]. BW25113 *E. coli* were made chemically
428 competent with the Hanahan method[61] and transformed with pKOCOMP encoding *adk*
429 from *Caldanaerobacter subterraneus* (Cs*adk*). Cell cultures were hereafter grown at
430 30 ºC unless otherwise stated. λ red recombination[62] was induced with 10 mM L-
431 arabinose, and induced cells were made electrocompetent and electroporated with a
432 chloramphenicol resistance cassette. Correct incorporation of the cassette was confirmed
433 by colony PCR using primers flanking the knocked out genomic *Ecadk* gene, and aliquots
434 of isolated clones from the resultant knockout strain were stored at -80 ºC as 20% (v/v)
435 glycerol stocks.
436
437 Cells from a frozen aliquot of the knockout strain were used to inoculate a culture of LB
438 with Cm + Amp and were made chemically competent[61] for transformation with pI-SceI.
439 The resultant strain BW25113 *adk::Cm* [pKOCOMP-Cs*adk*; pI-*SceI*] was hereafter
440 referred to as the "acceptor strain" (AS). Isolated clones from the AS were tested for
441 temperature and rhamnose sensitivity (for I-SceI induction) before storage as 20% (v/v)
442 glycerol stocks at -80 ºC.
443
444 A culture of 50 mL LB media was inoculated with cells from an AS glycerol stock (+ Cm,
445 Ap & Gm), supplemented with and 1% (w/v) glucose to prevent leaky I-*Sce*I expression.
446 The culture was grown to an OD_{600} of 0.5-0.6. Cells were harvested by centrifugation at
447 2,500 rcf for 10-15 min at room temperature, then washed twice in 20 mL of LB (+ Cm &
448 Gm). The culture was resuspended in 10 mL of LB (+ Cm & Gm) and used to inoculate
449 new 100 mL cultures of LB (+ Cm & Gm) to an OD_{600} of ~0.05. One culture was also
450 supplemented with ampicillin to serve as an uninduced control.
451
452 I-*Sce*I expression was induced by addition of 10 mM rhamnose to + Cm & Gm cultures
453 when they reached an OD_{600} between 0.1 and 0.15. The induced cultures were grown
454 until their growth started to slow relative to the uninduced control. Induced cultures were
455 then chilled on ice for 30-60 min. All following centrifugation steps were performed at 4 ºC
456 and cells were kept on ice. All solutions for washing were pre-chilled on wet ice. Cells
457 were pelleted by centrifugation for 10 min at 2,500 rcf and washed twice with 20 mL of
458 water (per 50 mL of culture). Cells were then resuspended and washed in 1 mL of water,
459 followed by 1 mL of 10% (v/v) glycerol, then resuspended in 200 µL of 10% (v/v) glycerol
460 per electroporation (typical OD_{600} ~30).
461

Electroporation was carried out in 2 mm gap cuvettes (Thermo Scientific #5520) pre-chilled on ice and with 500 ng DNA (either a homogeneous sample of WT *adk* or a heterogeneous sample of epPCR library). Cells were electroporated using a BioRad MicroPulser electroporator (EC2 setting) and immediately recovered with 800 µL of SOC media (New England Biolabs #B9020S). Qualitative pKOCOMP cleavage and negative controls were included by electroporating 2 µL of sterile water, each. Cultures were recovered in round-bottom tubes (Greiner Bio-One #187262) at 42 ºC with shaking at 220 rpm for 1.5 h. After recovery, the entire volume was used to inoculate 50 mL of LB (+ Cm, Gm, & glucose) in addition to 50 µg/mL kanamycin (+ Km), except for the pKOCOMP control culture, which was grown in the presence of 100 µg/mL ampicillin (+ Cm, Gm, Ap & glucose). Cultures were grown at 42 ºC with shaking at 220 rpm until reaching log phase. To check for pKOCOMP-positive clones, cultures were split to an OD_{600} of 0.2 into "+/- Ap media" (LB + Cm, Gm, Km, glucose, & +/- Ap). pKOCOMP depletion was deemed successful after a maximum of two splits. Resulting cultures were stored at -80 ºC as 15% (w/v) glycerol stocks. If the pKOCOMP-depleted culture was transformed with a WT *adk* it was plated at 42 ºC, and single clones were isolated and stored at -80 ºC as 15% (w/v) glycerol stocks. If the culture was transformed with an epPCR library, it was immediately used to inoculate a selection experiment.

In vivo selection experiments

In vivo selection experiments were performed in a Chi.Bio turbidostat (LABmaker, Berlin, Germany) with default settings unless otherwise stated[35]. Intrinsic turbidostat temperature control was aided by placing it in a Binder KB 115-UL incubator. All consumables (glass vials, stir bars, tubing, etc.) were purchased according to manufacturer's instructions (https://chi.bio/hardware/). Before use, chamber vials and stir bars were sterilized by autoclaving, and 3-port chamber caps with O-rings were sterilized with 70% (v/v) ethanol. Filled chambers were left to equilibrate to the selection temperature before blank measurements or inoculation. The medium for selection experiments was LB (+ Cm, Gm, Km & glucose) with the addition of 25 µg/mL nystatin as an antifungal. Chambers were inoculated to an OD_{600} of ~0.2 (OD_{650} ~0.35-0.5). Cultures were kept in mid log phase using OD_{650} regulation dithering between OD_{650} of 0.6 and 0.8 (set point 0.7). OD_{650} was measured every minute, and intervals between dilutions were fit to a single exponential using LMFIT[63] to calculate growth rate ($y = y_0 e^{rt}$ where y is OD_{600}, y_0 is initial OD_{600}, r is the growth rate, and t is time), then converted to a doubling time (DT) with the equation $DT = \frac{\ln(2)}{r}$. If the chamber vial was inoculated with a library, the remainder of that inoculation culture was miniprepped (Qiagen) and stored as a "42 ºC", or "pre-turbidostat" timepoint. Samples (6 mL) for genotyping were taken at least once per day and subsequently miniprepped and stored at -20 ºC. For flask experiments, cultures were inoculated to an OD_{600} of 0.2 and maintained at the selection temperature in an incubator (Infors HT Multitron AJ125) with shaking at 220 rpm. Cultures were maintained in log phase (OD_{600} 0.2-0.8) manually.

Nanopore sequencing

Sample preparation and data analysis for nanopore sequencing was adapted from Karst *et al*. using the longread_umi pipeline[36]. All primer sequences are included in

Supplementary Table 1. All PCR steps were performed using Invitrogen SuperFi DNA Polymerase (Invitrogen #12351010) and Invitrogen dNTP mix (Invitrogen #18427088).

1 ng of DNA was amplified in triplicate in a 50 µL PCR reaction to obtain a linear fragment starting 86 bp upstream of the promoter and ending 79 bp downstream of the *adk* gene. Reaction components: 1X SuperFi buffer, 1 mM dNTPs, 100 nM forward primer (pSFOXB15_ont_for), 100 nM reverse primer (pSFOXB15_ont_rev), 1 ng template DNA, 0.04 units/µL SuperFi Polymerase. PCR protocol: (1) initial denaturation for 30 sec at 98 ºC (2) 25 cycles of: (i) 98 ºC denaturation for 10 sec, (ii) 54 ºC annealing for 30 sec, (iii) 72 ºC extension for 35 sec, (3) 5 min final 72 ºC extension, (4) hold 10 ºC. All DNA purification steps were performed with a 0.5X volume ratio of AMPure resin (Beckman Coulter #A63881). Purified fragments were eluted in 30 µL of nuclease-free water (Invitrogen #AM9939). DNA concentration was quantified using Invitrogen Quant-iT dsDNA assay kits (Thermo Scientific #Q33130 and #Q33120), according to manufacturer's instructions, in opaque fluorescence 96-well plates (Corning 3993) with a SpectraMax i3x Microplate reader (Molecular Devices) or a BioTek Cytation5 Reader (Agilent). Next, each fragment was diluted to 50,000 molecules/µL (for timepoints) or 250,000 molecules/µL (for unselected libraries) and barcoded on both ends with unique molecular identifiers (UMIs) in a 50 µL PCR reaction. Reaction components: 1X SuperFi buffer, 1 mM dNTPs, 500 nM forward primer (ont_ss_dumi_for), 500 nM reverse primer (ont_ss_dumi_rev), 50,000-250,000 molecules template DNA, 0.04 units/µL SuperFi Polymerase. PCR protocol: (1) initial denaturation for 30 sec at 98 ºC, (2) 2 cycles of (i) 98 ºC denaturation for 10 sec, (ii) 55 ºC annealing for 30 sec, (iii) 72 ºC extension for 35 sec, (3) hold at 10 ºC. Tagged fragments were purified and eluted in 20 µL of nuclease-free water. The entire eluate was used as the template in a 100 µL PCR reaction. Reaction components: 1X SuperFi buffer, 1 mM dNTPs, 250 nM forward primer, 250 nM reverse primer, 1 ng template DNA, 0.04 units/µL SuperFi Polymerase. PCR protocol: (1) initial denaturation for 30 sec at 98 ºC, (2) 25 cycles of (i) 98 ºC denaturation for 10 sec, (ii) 60 ºC annealing for 30 sec, (iii) 72 ºC extension for 35 sec, (3) 5 min final 72 ºC extension, (4) hold 10 ºC. 2 ng of the purified PCR product was re-amplified via the same PCR protocol to obtain sufficient yield for long-read sequencing.

Custom Sequencing was performed by Plasmidsaurus using Oxford Nanopore Technology to a target depth of 33X with custom analysis and annotation. The basecalled fastq files were analyzed using the longread_umi pipeline[36]. The output list of consensus sequences was filtered for a depth of ≥ 15X and the remaining sequences were aligned to the WT sequence using MAFFT command line wrapper [64] module in Biopython [65] with settings auto=True, inputorder=True, jtt=1, tm=2, op=1.53, ep-0.123, quiet=False. This alignment was used to extract regions from each amplicon (*e.g.,* promoter, 5′ UTR, KSD, *adk*, 5′ UTR) for easy comparison. The *adk* region of each variant was then translated using Biopython and pairwise aligned to the WT sequence for naming variants in the format w#m (w=WT ID, #=residue number, m=mutation ID). Contaminating Adk sequences were identified and removed by string comparison using RapidFuzz.[66] Frequency of each unique Adk variant on the amino acid level was calculated by dividing the abundance of each variant by the total number of variants.

553 **Adk large scale expression**
554 All *adk* overexpression constructs were designed with a C-terminal tobacco etch virus
555 (TEV) protease cleavage/recognition site and octahistidine tag (*adk-TEV-His$_8$*).
556 Sequences were codon optimized for expression in *E. coli*, synthesized, and cloned into
557 pET-17b by GenScript using restriction sites HindIII and KpnI. A pilot culture of LB
558 supplemented with 100 µg/mL ampicillin was inoculated with 1 colony of BL21 (DE3)
559 Competent *E. coli* (New England Biolabs) transformed with pET-17b-*adk-TEV-His$_8$* and
560 grown at 37 ºC overnight with shaking at 220 rpm. 1-6 L of LB supplemented with
561 100 µg/mL ampicillin were inoculated with 20 mL/L of pilot culture and grown at 37 ºC with
562 shaking at 220 rpm until an OD_{600} of 0.6-0.8 at which point *adk-TEV-His$_8$* expression was
563 induced with 1 mM isopropyl β-D-1-thiogalactopyranoside (IPTG) for 4 h at 37 ºC. Cells
564 were harvested by centrifugation at 4,000 rpm for 15-20 min in a JLA-8.1000 rotor
565 (Beckman Coulter) and stored at -20 ºC until purification.
566
567 **Adk 96-well plate expression**
568 BL21 (DE3) Competent *E. coli* (New England Biolabs) were transformed with 50 ng of
569 pET-17b epPCR library according to manufacturer's instructions. Alongside the libraries,
570 two additional BL21 aliquots were transformed with 50 ng of pET-17b encoding WT *adk-*
571 *TEV-His$_8$* or a catalytically inactive variant, *adkR88K-TEV-His$_8$*. 10-50 µL of recovered
572 transformation were plated on LB agar plates (100 µg/mL ampicillin) to obtain well-
573 isolated colonies. All cell growth was done in Thermo Scientific™ Nunc™ Edge™ 96-well,
574 nunclon delta-treated flat-bottomed microplates (Thermo Scientific #167542) with 200 µL
575 of LB supplemented with 100 µg/mL ampicillin. Wells were covered with CELLTREAT
576 breathable sealing film and incubated in a MB-100 thermo-shaker. A pilot culture 96-well
577 plate was inoculated with 1 colony per well (84 library variants, 6 WT, and 6 R88K) with
578 controls distributed randomly across each plate. The pilot plate was grown overnight at
579 37 ºC with shaking at 600 rpm. The next day, an expression plate was inoculated with
580 5 µL of pilot culture. Remaining pilot cultures were preserved as ~10% (v/v) glycerol
581 stocks at -80 ºC. The expression plate was grown at 37 ºC with shaking at 600 rpm until
582 the average plate OD_{600} reached 0.8. All OD_{600} measurements were performed using a
583 BioTek Cytation5 Reader (Agilent). Expression was induced in every well with 1 mM
584 isopropyl β-D-1-thiogalactopyranoside (IPTG) for 4 h at 37 ºC. OD_{600} of 5-fold diluted
585 wells was measured to correct for cell content during data analysis. Cells were harvested
586 by centrifugation at 1,500 rcf for 10-15 min and stored at -20 ºC.
587
588 **Purification of Adk large-scale expressions**
589 All purification steps took place at 4 ºC. Cell pellets from *adk-TEV-His$_8$* overexpression
590 were resuspended in ~20 mL of lysis buffer per gram of cell pellet. Lysis buffer was Buffer
591 A (50 mM Tris, 300 mM NaCl, 2.5 mM β-mercaptoethanol, pH 7.5) supplemented with 1X
592 Halt Protease inhibitor cocktail, deoxyribonuclease, and lysozyme. Resuspended cells
593 were lysed by sonication for 10 min (20 sec on, 40 sec off, power output ≤ 40 W) and
594 cleared by centrifugation in a JA-20 rotor (Beckman Coulter) pre-chilled to 4 ºC at
595 18,000 rpm for 30-45 min.
596
597 The His-tagged Adk was purified via nickel-affinity chromatography on an Äkta Start.
598 Lysate was loaded at 1-2 mL/minute on a HisTrap column (Cytiva) pre-equilibrated in

599 Buffer A and the column was washed with Buffer A until the UV (280 nm) baselined.
600 Subsequent wash steps were performed at 4 mL/min. To remove bound nucleotides, the
601 column was washed with 10 column volumes (CV) of Buffer B (50 mM Tris, 1 M NaCl,
602 2.5 mM β-mercaptoethanol, pH 7.5). Nonspecifically bound contaminants were removed
603 by washing with 5-10 CV of Buffer C (50 mM Tris, 300 mM NaCl, 25 mM imidazole,
604 2.5 mM β-mercaptoethanol, pH 7.5). His-tagged Adk was eluted with Buffer D (50 mM
605 Tris, 300 mM NaCl, 500 mM imidazole, 2.5 mM β-mercaptoethanol, pH 7.5). His-tagged
606 TEV protease[67] was added to the eluate in a 1:30 TEV:total protein ratio and the sample
607 was dialyzed overnight against 2 L of Buffer A per 30 mL of eluate in a 10 kDa MWCO
608 Slide-A-Lyzer G2 dialysis cassette (Thermo Scientific).
609
610 The dialysate was filtered through a Whatman 0.2 µm PES membrane and loaded back
611 onto the HisTrap column to separate cleaved Adk from the tag and TEV protease.
612 Cleaved Adk was collected in the flow-through. Purity of Adk fractions and confirmation
613 of successful tag cleavage by TEV protease was assessed by SDS PAGE. Adk was
614 further purified via gel filtration on a Superdex S75 pg 16/60 or 16/600 (Cytiva) connected
615 to an Äkta Pure and equilibrated in Buffer E (40 mM MOPS, 50 mM NaCl, 2 mM TCEP,
616 pH 7.0). Purified fractions containing Adk were combined and concentrated, if necessary,
617 in an Amicon Ultra-15 10 kDa MWCO centrifugal filter to a concentration < 1 mM.
618 Samples were flash frozen in liquid nitrogen and stored at -80 ºC.
619
620 **Batch purification of Adk small-scale expressions**
621 Cell pellets from 1 L *adk-TEV-His$_8$* expressions were resuspended in 20 mL of Buffer A
622 (40 mM MOPS, 300 mM NaCl, 2.5 mM β-mercaptoethanol, pH 7) supplemented with 1X
623 Halt protease inhibitor cocktail, deoxyribonuclease, and lysozyme. Resuspended cells
624 were lysed by sonication using a microtip for 2 min (20 sec on, 40 sec off, power output
625 ≤ 21 W). Lysate was cleared by centrifugation in a JA-14.5 rotor (Beckman Coulter) pre-
626 chilled to 4 ºC for 1 h at 8,000 rpm. His-tagged Adk was purified in batch by cobalt affinity.
627 Cleared lysate was filtered directly onto 5 mL of TALON affinity resin (Takara Bio) pre-
628 equilibrated in Buffer A, then incubated for 1 h with gentle agitation at 80 rpm in a shaking
629 incubator (Infors HT Multitron AJ125) at 15 ºC or on a rotating platform at room
630 temperature.
631
632 All centrifugation steps were performed for 5-10 min at 3,000 rcf and 10 ºC. After
633 decanting the supernatant, the resin was washed in > 10 CV of Buffer B (40 mM MOPS,
634 1 M NaCl, 2.5 mM β-mercaptoethanol, pH 7.0) to remove bound nucleotides.
635 Nonspecifically bound proteins were washed with > 10 CV of Buffer C (40 mM MOPS,
636 300 mM NaCl, 5 mM imidazole, 2.5 mM β-mercaptoethanol, pH 7.0). The resin was
637 washed then with > 10 CV of Buffer A to remove all imidazole, resuspended in 1 mL of
638 Buffer A, and an on-resin tag cleavage was initiated by adding 300 µg of His-tagged TEV
639 protease[67]. Cleavage proceeded at 4 ºC overnight with gentle agitation on a rotating
640 platform.
641
642 Cleavage and purity were assessed via SDS-PAGE. Samples were always ≥ 95% pure
643 (data not shown). The samples were then filtered with a Whatman 0.2 µm PES membrane
644 to remove residual resin and slowly mixed with a concentrated stock of TCEP (250-

500 mM) in Buffer A to preserve reducing agent in the samples. The samples were concentrated in Amicon Ultra-0.5 10 kDa MWCO centrifugal filters (Millipore Sigma) to concentrations ranging from 200-500 μM. Precipitated debris was removed by centrifuging each sample at 10 ºC for 10 min at 14,000 rcf and transferring the supernatant into a new tube. Batch-purified Adks occasionally had high 260/280 values when measured by NanoDrop (Thermo Scientific NanoDrop One Microvolume UV-Vis Spectrophotometer or NanoDrop 2000c), thereby making A_{280} readings inaccurate, so a Bradford assay (Thermo Scientific #A55866) was used to quantify protein concentration for these samples. The purified samples were then assayed immediately, after which they were flash frozen in liquid nitrogen and stored at -80 ºC.

Coupled assay of purified Adk

Enzymatic activity of Adks was measured in triplicate using a spectroscopic assay coupled to the reduction of nicotinamide adenine dinucleotide phosphate ($NADP^+$ to NADPH). NADPH formation was measured at 340 nm using either a SpectraMax i3x Microplate Reader (Molecular Devices) or a BioTek Cytation5 Reader (Agilent). Assay buffer was 40 mM MOPS, 80 mM KCl, pH 7.0. Assays were performed in a 100 μL volume containing 10 units of hexokinase from yeast (Millipore Sigma), 10 units of glucose-6-phosphate dehydrogenase from *Leuconostoc mesenteroides* (Fisher Scientific), 0.5 mM $NADP^+$, 5 mM glucose, 5 mM $MgCl_2$, 5 mM adenosine diphosphate (ADP), 0.3 mg/mL bovine serum albumin (BSA), and 1-5 nM Adk in assay buffer. A master mix containing assay buffer, hexokinase, glucose-6-phosphate dehydrogenase, $NADP^+$, and BSA was incubated in a covered microplate (Corning 3994) at the assay temperature for ≥ 15 min. After incubation, glucose and then Mg^{2+}•ADP were added to each well. All reagents were also incubated at the assay temperature for ≥ 15 min. Between addition of each reagent there was an additional incubation period of 5 min, during which a baseline A_{340} measurement was recorded. The reaction was initiated with Adk and measured for 30 min. Background reactions were “initiated” with buffer instead of Adk and subtracted from + Adk data. The linear portion of each reaction was used to calculate a slope of NADPH formation vs. time using the correction coefficient 0.0032 or 0.0031 $\mu M^{-1}cm^{-1}$ for the SpectraMax and Cytation5 plate readers, respectively, and divided by Adk concentration to calculate a k_{cat}.

Coupled assay of acceptor strain expressing Adk variants

Triplicate samples containing 5 x 10^7 cells were pelleted by centrifugation for 5 min at 5,000 rcf (4 ºC). Pellets were resuspended in 1 mL of assay buffer and sonicated for 20 sec using a microtip (10 sec on, 20 sec off, power output ≤ 15 W) then cleared by centrifugation at 4 ºC for 30 min at 16,900 rcf. 40 μL of lysate per reaction was used in the assay. The coupled assay was performed similarly as to what was described for purified Adks, but with 1 mM $NADP^+$, and lysate was incubated with the master mix and so the reaction was initiated by addition of Mg^{2+}•ADP. 500 μM of the Adk inhibitor P^1,P^5-Di(adenosine-5′) pentaphosphate (Ap5A) was also included for lysates as a negative control for basal lysate activity. The linear portion of each reaction was used to calculate a slope of NADPH formation vs. time using the correction coefficient 0.0032 or 0.0031 $\mu M^{-1}cm^{-1}$ for the SpectraMax and Cytation5 plate readers, respectively, and background-corrected slopes were divided by the k_{cat} to calculate in-cell Adk concentration.

691
692 **Coupled assay for *in vitro* lysate screen**
693 To prepare *in vitro* lysates, each sample was resuspended in 40 µL of 1X BugBuster
694 (Millipore Sigma) diluted in assay buffer and incubated at room temperature with shaking
695 in a MB-100 thermo-shaker at 600 rpm for 1 h. The lysate was cleared by centrifugation
696 at 1,500 rcf (4 ºC) for 10-15 min and 10 µL of 1/4,900-fold diluted lysate was used in
697 activity assays.
698
699 The coupled assay was performed similarly as to what was described for purified Adks,
700 but with 1 mM $NADP^+$, and lysate was incubated with the master mix and so the reaction
701 was initiated by addition of Mg^{2+}•ADP. Wells expressing the catalytically dead R88K
702 variant were used as negative controls for basal lysate activity. The linear portion of each
703 reaction was used to calculate a slope of NADPH formation vs. time using the correction
704 coefficient 0.0032 or 0.0031 $\mu M^{-1}cm^{-1}$ for the SpectraMax and Cytation5 plate readers,
705 respectively, and background-corrected slopes were divided by the final measured OD_{600}
706 to correct for cell content per well. All velocities were normalized to WT activity. Only wells
707 that were induced at OD_{600} between 0.2-1 were analyzed to reduce false negatives from
708 variants that did not express well due to being induced at an OD_{600} that was too low or
709 too high. For wells that were genotyped, Adk concentrations were calculated by dividing
710 the velocities by k_{cat}.
711
712 **Discontinuous HPLC assay**
713 High-pressure liquid chromatography (HPLC) assays to assess activity-temperature
714 profiles were performed from 10-90 ºC (10 ºC increments). Adk was pre-incubated for
715 15 min at target temperature before reaction initiation with 5 mM Mg^{2+}•ADP. Between 10-
716 40 ºC, 10 nM and 20 nM of ANC2 and AfAdk, respectively, were used and between 50-
717 90 ºC 5 nM and 10 nM of ANC2 and AfAdk, respectively. 10 µL timepoints (20, 40, 60, 90,
718 and 120 s) at each temperature were collected and quenched with 10% (v/v) TCA (10 µL)
719 and cleared by centrifuging in a Spin-X centrifugal tube filter (Costar #8160) for 10 min at
720 5,000 rpm. The pH was neutralized by addition of 20 µL of 1.5 mM HEPES, pH 8.0.
721 Samples were stored at -20 ºC until analysis.
722
723 Nucleotide amounts in each sample were analyzed using an HPLC system (Agilent
724 Infinity 1260) with an analytical HPLC column (ACE; EXL-129-2502U, i.d. 2.1 mm, length
725 250 mm, C18-AR, 5 Å pore size). Isocratic elution with a 100 mM potassium phosphate,
726 pH 6.0 mobile phase was used for nucleotide separation. ATP, ADP, and AMP were
727 individually integrated (ChemStation) and their ratios were used to calculate nominal
728 concentration considering a total of 5 mM of nucleotides. The reaction velocity at each
729 temperature was determined by linear regression (Prism 10.1.1 GraphPad Software) of
730 ATP production over time and k_{cat} was calculated by dividing velocity by enzyme
731 concentration. Depicted errors are the propagated standard error of the slope obtained
732 from linear regression. Control experiments using only buffer or Mg^{2+}•ADP were
733 performed to examine residual contaminants.
734
735 **Determination of melting temperatures**

Melting temperatures were determined using a thermal shift assay conducted in a QuantStudio 3 Real-Time PCR System (Applied Biosystems) according to manufacturer's instructions. 5-20 μM of Adk was combined with 5X SYPRO Orange (Invitrogen #S6650) in assay buffer (20 μL total volume) in a MicroAmp Optical 96-well reaction plate (Applied Biosystems #N8010560). Melt curves were generated by measuring fluorescence intensity from 20-95 ºC. The inflection point of the melting curve was used to determine the melting temperature.

References

1. Linus Pauling, Emile Zuckerkandl, Thormod Henriksen, & Rolf A. Løvstad. Chemical Paleogenetics. Molecular 'Restoration Studies' of Extinct Forms of Life. *Acta Chemica Scandinavica* https://doi.org/10.3891/acta.chem.scand.17s-0009 (1963) doi:10.3891/acta.chem.scand.17s-0009.
2. Finnigan, G. C., Hanson-Smith, V., Stevens, T. H. & Thornton, J. W. Evolution of increased complexity in a molecular machine. *Nature* **481**, 360–364 (2012).
3. Schulz, L. *et al.* Evolution of increased complexity and specificity at the dawn of form I Rubiscos. *Science* **378**, 155–160 (2022).
4. Hadzipasic, A. *et al.* Ancient origins of allosteric activation in a Ser-Thr kinase. *Science* **367**, 912–917 (2020).
5. Nguyen, V. *et al.* Evolutionary drivers of thermoadaptation in enzyme catalysis. *Science* **355**, 289–294 (2017).
6. Prakinee, K., Phaisan, S., Kongjaroon, S. & Chaiyen, P. Ancestral Sequence Reconstruction for Designing Biocatalysts and Investigating their Functional Mechanisms. *JACS Au* **4**, 4571–4591 (2024).
7. Whitfield, J. H. *et al.* Construction of a robust and sensitive arginine biosensor through ancestral protein reconstruction. *Protein Science* **24**, 1412–1422 (2015).
8. Schriever, K. *et al.* Engineering of Ancestors as a Tool to Elucidate Structure, Mechanism, and Specificity of Extant Terpene Cyclase. *J. Am. Chem. Soc.* **143**, 3794–3807 (2021).
9. Babkova, P., Sebestova, E., Brezovsky, J., Chaloupkova, R. & Damborsky, J. Ancestral Haloalkane Dehalogenases Show Robustness and Unique Substrate Specificity. *ChemBioChem* **18**, 1448–1456 (2017).
10. Gutierrez-Rus, L. I. *et al.* Ancestral versus Modern Substrate Scope in Family-1 Glycosidases. *bioRxiv* 2024.04.11.589065 (2024) doi:10.1101/2024.04.11.589065.
11. Keser, M. *et al.* Stable and Promiscuous Galactose Oxidases Engineered by Directed Evolution, Atomistic Design, and Ancestral Sequence Reconstruction. *ACS Synth. Biol.* **14**, 239–246 (2025).
12. Spence, M. A., Kaczmarski, J. A., Saunders, J. W. & Jackson, C. J. Ancestral sequence reconstruction for protein engineers. *Current Opinion in Structural Biology* **69**, 131–141 (2021).
13. Alcalde, M. When directed evolution met ancestral enzyme resurrection. *Microb. Biotechnol.* **10**, 22–24 (2017).
14. Tokuriki, N. & Tawfik, D. S. Protein Dynamism and Evolvability. *Science* **324**, 203–207 (2009).

15. Tokuriki, N. & Tawfik, D. S. Stability effects of mutations and protein evolvability. *Current Opinion in Structural Biology* **19**, 596–604 (2009).
16. Goldsmith, M. & Tawfik, D. S. Enzyme engineering: reaching the maximal catalytic efficiency peak. *Current Opinion in Structural Biology* **47**, 140–150 (2017).
17. Gomez-Fernandez, B. J. *et al.* Directed -in vitro- evolution of Precambrian and extant Rubiscos. *Scientific Reports* **8**, 5532 (2018).
18. Risso, V. A. *et al.* De novo active sites for resurrected Precambrian enzymes. *Nature Communications* **8**, 16113 (2017).
19. Gumulya, Y. *et al.* Engineering highly functional thermostable proteins using ancestral sequence reconstruction. *Nature Catalysis* **1**, 878–888 (2018).
20. Tokuriki, N. & Tawfik, D. S. Stability effects of mutations and protein evolvability. *Curr. Opin. Struct. Biol.* **19**, 596–604 (2009).
21. Cole, M. F. & Gaucher, E. A. Utilizing natural diversity to evolve protein function: applications towards thermostability. *Current Opinion in Chemical Biology* **15**, 399–406 (2011).
22. Bershtein, S., Segal, M., Bekerman, R., Tokuriki, N. & Tawfik, D. S. Robustness–epistasis link shapes the fitness landscape of a randomly drifting protein. *Nature* **444**, 929–932 (2006).
23. Hart, K. M. *et al.* Thermodynamic System Drift in Protein Evolution. *PLOS Biology* **12**, e1001994 (2014).
24. Tokuriki, N. & Tawfik, D. S. Chaperonin overexpression promotes genetic variation and enzyme evolution. *Nature* **459**, 668–673 (2009).
25. Goldenzweig, A. *et al.* Automated Structure- and Sequence-Based Design of Proteins for High Bacterial Expression and Stability. *Molecular Cell* **63**, 337–346 (2016).
26. Goldenzweig, A. & Fleishman, S. Principles of Protein Stability and Their Application in Computational Design. *Annu. Rev. Biochem.* **87**, 1–25 (2018).
27. Wagner, A. Robustness and evolvability: a paradox resolved. *Proceedings of the Royal Society B: Biological Sciences* **275**, 91–100 (2007).
28. Bloom, J. D., Labthavikul, S. T., Otey, C. R. & Arnold, F. H. Protein stability promotes evolvability. *Proceedings of the National Academy of Sciences* **103**, 5869–5874 (2006).
29. Wheeler, L. C., Lim, S. A., Marqusee, S. & Harms, M. J. The thermostability and specificity of ancient proteins. *Current Opinion in Structural Biology* **38**, 37–43 (2016).
30. Harms, M. J. & Thornton, J. W. Evolutionary biochemistry: revealing the historical and physical causes of protein properties. *Nature Reviews Genetics* **14**, 559–571 (2013).
31. Trudeau, D. L., Kaltenbach, M. & Tawfik, D. S. On the Potential Origins of the High Stability of Reconstructed Ancestral Proteins. *Molecular Biology and Evolution* **33**, 2633–2641 (2016).
32. Couñago, R., Chen, S. & Shamoo, Y. In Vivo Molecular Evolution Reveals Biophysical Origins of Organismal Fitness. *Molecular Cell* **22**, 441–449 (2006).
33. Couñago, R. & Shamoo, Y. Gene replacement of adenylate kinase in the gram-positive thermophile Geobacillus stearothermophilus disrupts adenine nucleotide homeostasis and reduces cell viability. *Extremophiles* **9**, 135–144 (2005).
34. Billerbeck, S. & Panke, S. A genetic replacement system for selection-based engineering of essential proteins. *Microbial Cell Factories* **11**, 110 (2012).

35. Steel, H., Habgood, R., Kelly, C. L. & Papachristodoulou, A. In situ characterisation and manipulation of biological systems with Chi.Bio. *PLOS Biology* **18**, e3000794 (2020).
36. Karst, S. M. *et al.* High-accuracy long-read amplicon sequences using unique molecular identifiers with Nanopore or PacBio sequencing. *Nature Methods* **18**, 165–169 (2021).
37. Henzler-Wildman, K. A. *et al.* A hierarchy of timescales in protein dynamics is linked to enzyme catalysis. *Nature* **450**, 913–916 (2007).
38. Kerns, S. J. *et al.* The energy landscape of adenylate kinase during catalysis. *Nature Structural & Molecular Biology* **22**, 124–131 (2015).
39. Couñago, R. & Shamoo, Y. Gene replacement of adenylate kinase in the gram-positive thermophile Geobacillus stearothermophilus disrupts adenine nucleotide homeostasis and reduces cell viability. *Extremophiles* **9**, 135–144 (2005).
40. Couñago, R., Chen, S. & Shamoo, Y. In Vivo Molecular Evolution Reveals Biophysical Origins of Organismal Fitness. *Molecular Cell* **22**, 441–449 (2006).
41. Kim, J. *et al.* Hidden resources in the Escherichia coli genome restore PLP synthesis and robust growth after deletion of the essential gene pdxB. *Proceedings of the National Academy of Sciences* **116**, 24164–24173 (2019).
42. Peña, M. I., Davlieva, M., Bennett, M. R., Olson, J. S. & Shamoo, Y. Evolutionary fates within a microbial population highlight an essential role for protein folding during natural selection. *Molecular Systems Biology* **6**, 387 (2010).
43. Arnold, F. H. Directed Evolution: Bringing New Chemistry to Life. *Angewandte Chemie International Edition* **57**, 4143–4148 (2018).
44. Payne, J. L. & Wagner, A. The causes of evolvability and their evolution. *Nature Reviews Genetics* **20**, 24–38 (2019).
45. Starr, T. N., Picton, L. K. & Thornton, J. W. Alternative evolutionary histories in the sequence space of an ancient protein. *Nature* **549**, 409–413 (2017).
46. Xie, V. C., Pu, J., Metzger, B. P., Thornton, J. W. & Dickinson, B. C. Contingency and chance erase necessity in the experimental evolution of ancestral proteins. *eLife* **10**, e67336 (2021).
47. Metzger, B. P. H., Park, Y., Starr, T. N. & Thornton, J. W. Epistasis facilitates functional evolution in an ancient transcription factor. *eLife* https://doi.org/10.7554/elife.88737.2 (2024) doi:10.7554/elife.88737.2.
48. Fröhlich, C. *et al.* Epistasis arises from shifting the rate-limiting step during enzyme evolution of a β-lactamase. *Nature Catalysis* **7**, 499–509 (2024).
49. Bridgham, J. T., Ortlund, E. A. & Thornton, J. W. An epistatic ratchet constrains the direction of glucocorticoid receptor evolution. *Nature* **461**, 515–519 (2009).
50. Williams, P. D., Pollock, D. D., Blackburne, B. P. & Goldstein, R. A. Assessing the Accuracy of Ancestral Protein Reconstruction Methods. *PLoS Computational Biology* **2**, e69 (2006).
51. Susko, E. & Roger, A. J. Problems With Estimation of Ancestral Frequencies Under Stationary Models. *Systematic Biology* **62**, 330–338 (2013).
52. Sternke, M., Tripp, K. W. & Barrick, D. Chapter Seven The use of consensus sequence information to engineer stability and activity in proteins. *Methods in Enzymology* **643**, 149–179 (2020).

53. Akanuma, S. & Yamagishi, A. Biotechnology of Extremophiles:, Advances and Challenges. *Grand Challenges in Biology and Biotechnology* 581–596 (2016) doi:10.1007/978-3-319-13521-2_20.
54. Akanuma, S. *et al.* Experimental evidence for the thermophilicity of ancestral life. *PNAS* **110**, 11067–11072 (2013).
55. McKinney, W. Data Structures for Statistical Computing in Python. in *Proceedings of the 9th Python in Science Conference* (eds Walt, S. van der & Millman, J.) 56–61 (2010). doi:10.25080/Majora-92bf1922-00a.
56. Harris, C. R. *et al.* Array programming with NumPy. *Nature* **585**, 357–362 (2020).
57. Virtanen, P. *et al.* SciPy 1.0: fundamental algorithms for scientific computing in Python. *Nature Methods* **17**, 261–272 (2020).
58. J. D. Hunter. Matplotlib: A 2D Graphics Environment. *Computing in Science & Engineering* **9**, 90–95 (2007).
59. Abramson, J. *et al.* Accurate structure prediction of biomolecular interactions with AlphaFold 3. *Nature* **630**, 493–500 (2024).
60. Goddard, T. D. *et al.* UCSF ChimeraX: Meeting modern challenges in visualization and analysis. *Protein Science* **27**, 14–25 (2018).
61. Hanahan, D. Studies on transformation of Escherichia coli with plasmids. *Journal of molecular biology* **166**, 557–580 (1983).
62. Datsenko, K. A. & Wanner, B. L. One-step inactivation of chromosomal genes in Escherichia coli K-12 using PCR products. *Proceedings of the National Academy of Sciences* **97**, 6640–6645 (2000).
63. Newville, M. *et al.* LMFIT: Non-Linear Least-Squares Minimization and Curve-Fitting for Python. https://doi.org/10.5281/zenodo.598352 doi:10.5281/zenodo.598352.
64. Katoh, K. & Toh, H. Recent developments in the MAFFT multiple sequence alignment program. *Briefings in Bioinformatics* **9**, 286–298 (2008).
65. Cock, P. J. A. *et al.* Biopython: freely available Python tools for computational molecular biology and bioinformatics. *Bioinformatics* **25**, 1422–1423 (2009).
66. Bachmann, M. rapidfuzz/RapidFuzz: Release 3.8.1. Zenodo https://doi.org/10.5281/zenodo.10938887 (2024).
67. Keeble, A. H. *et al.* DogCatcher allows loop-friendly protein-protein ligation. *Cell Chemical Biology* **29**, 339-350.e10 (2022).

Data Availability

The data that support the findings of this study are available from the corresponding author upon reasonable request.

Acknowledgements: We would like to thank Michael Sennett, Ricardo Pádua, Lufan Xiao and other members of the Kern lab for valuable discussions. Additionally, we are grateful for the help of Steven Panke and Søren Karst with establishing their nanopore data analysis pipeline on our high-performance computing cluster as well as advice from Steve Harrison concerning the Chi.Bio turbidostat. This work was supported by the Howard Hughes Medical Institute (HHMI) to Dorothee Kern.

Competing Interests. D.K. is a co-founder of Relay Therapeutics and MOMA Therapeutics. H. L. and D.K. are listed as inventors on Patent PCT/US2025/021803

WO2025207918A1 related to the methods described in this manuscript. The remaining authors declare no competing interests.

Author contributions:

M.P., H.L., C.W., D.R.W., C.K., D.L.T., and D.K. contributed to the design and conceptualization of the project. M.P., H.L., C.W., D.R.W., and C.K. made knockout and WT knock-in cell strains. M.P., H.L., D.R.W., C.K., and J.I. measured WT acceptor strain doubling times. M.P. made error-prone PCR libraries. M.P. and H.L. performed *in vivo* experiments. M.P. prepared and analyzed all nanopore sequencing data. M.P. performed *in vitro* selection experiments. M.P., H.L., C.K., and A.U. expressed, purified, and measured enzymatic activity and thermostability WT and variant Adks. M.P., H.L., C.K., and A.U. expressed, purified, and measured enzymatic activity and thermostability WT and variant Adks. H.L. performed the HPLC assay of Adks. M.P., H.L., and D.K. wrote the manuscript. All authors reviewed the manuscript.

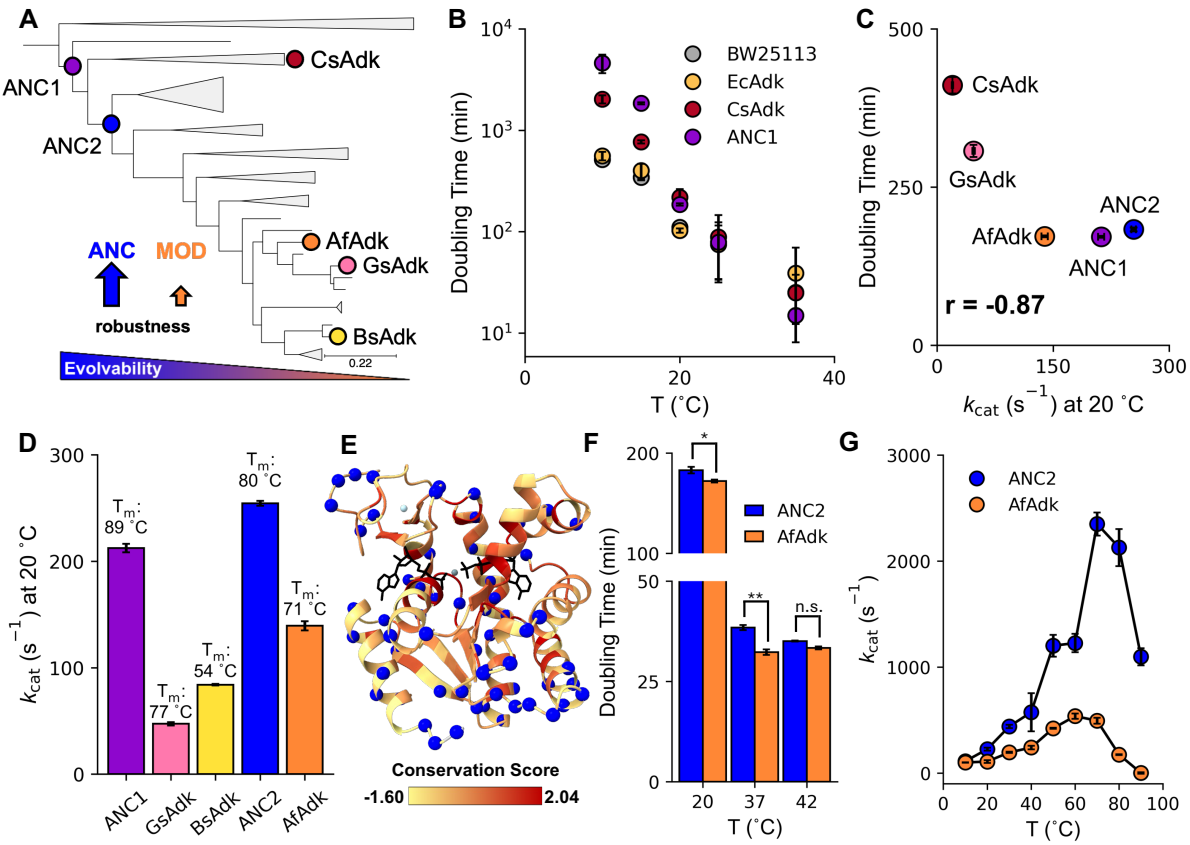

Fig. 1: ANC2 and AfAdk are the most comparable ancestral/extant pair for *in vivo* directed evolution at low temperature. A Collapsed phylogenetic tree taken from Nguyen *et al.* (2017)[5] is shown annotated with ancestral and modern Adks used in this study (Ancestor 1: ANC1, Ancestor 2: ANC2, *Caldanaerobacter subterraneus*: CsAdk, *Anoxybacillus flavithermus*: AfAdk, *Geobacillus stearothermophilus*: GsAdk, *Bacillus subtilis*: BsAdk). The hypothesized relationship between evolvability and robustness is illustrated. **B** Doubling times of *Escherichia coli* Adk (EcAdk) knockout *E. coli* BW25113 strains supplemented with indicated Adk variants on a placeholder plasmid at different temperatures. **C** Doubling times at 20 ºC of knockout strains rescued with different *adks* strongly correlate with the k_{cat} of the rescue Adk (Pearson r = -0.87) indicating that Adk activity is rate-limiting for *E. coli* growth. **D** k_{cat} of Adk-catalyzed ATP production from 5 mM Mg^{2+}•2ADP measured at 20 ºC, via coupled assay (mean ± s.d. of n ≥ 3 replicates) and respective melting temperature T_m (indicated above the bar) show ANC2 and AfAdk as closest-matching ancestor-extant pair. **E** AlphaFold 3 prediction of AfAdk (cartoon) bound to Mg^{2+}•ADP colored by the sequence conservation score of Adks found in the phylogenetic tree. Sequence differences between AfAdk and ANC2 are displayed as blue spheres (sequence ID 72.4%). Mg^{2+} (slate) and Zn^{2+} (light blue) are depicted as small spheres and ADP (black) as black sticks. **F** Temperature dependence of doubling times of the acceptor strain (AS; mean ± s.e. of n ≥ 3 replicates) rescued with WT ANC2 or AfAdk at different temperatures (Kolmogorov-Smirnov test, $p_{20ºC}$ = 0.03, $p_{37ºC}$ = 0.001, $p_{42ºC}$ = 0.8; *: p < 0.05, **: p < 0.01, n.s.: not significant). **G** k_{cat} of ATP production from Mg^{2+}•2ADP at different temperatures measured via high-pressure liquid chromatography (HPLC). All k_{cat} values are the average of n ≥ 3 replicate measurements ± s.e.

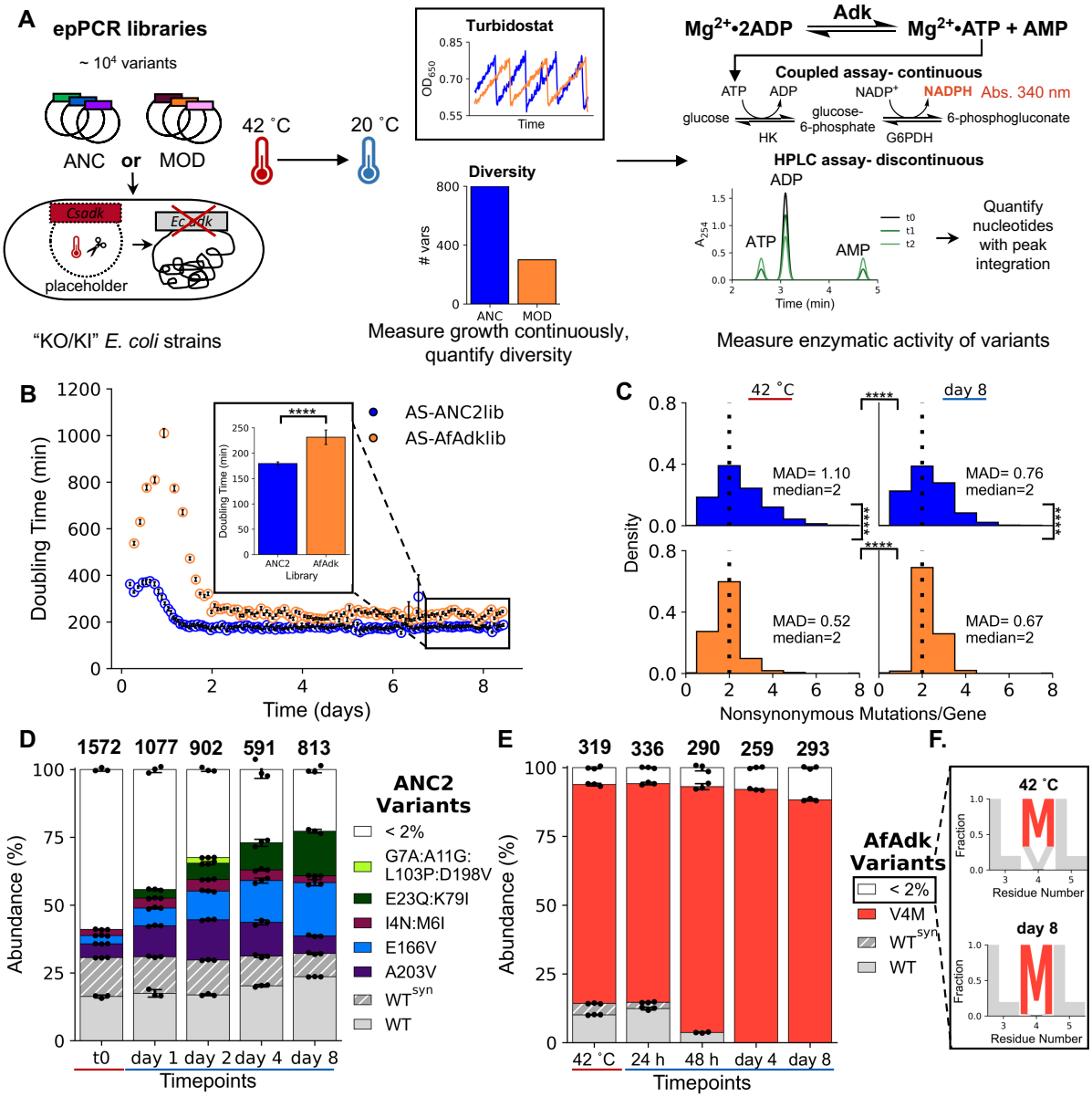

Fig. 2: ANC2 is more robust to mutation than AfAdk at 20 ºC *in vivo*. A Scheme of the experimental setup for *in vivo* selection of acceptor strains rescued with ancestral or modern epPCR libraries, ensuring continuous bacterial growth in log phase and continuous doubling time measurement using the Chi.Bio turbidostat[35]. Readouts for robustness are the number of viable variants, and two methods used to measure k_{cat} for winners are shown. **B** Doubling times of AS-ANC2lib and AS-AfAdklib strains throughout 8 days of selection at 20 ºC in turbidostat, revealing a significantly faster growth of the ancestral libraries than modern libraries (Kolmogorov-Smirnov test, $p = 1.9 \times 10^{-31}$), with an initial 2-day adaptation phase. **C** Histograms display significantly larger genetic diversity (mutations/gene) in ancestors than moderns before (at 42 ºC) and after 8 days of selection at 20 ºC (Kolmogorov-Smirnov tests: $p_{ANC2} = 1.04 \times 10^{-5}$, $p_{AfAdk} = 7.04 \times 10^{-16}$, $p_{ANC2,AfAdk,42ºC} = 2.11 \times 10^{-38}$, $p_{ANC2,AfAdk,day8} = 5.62 \times 10^{-15}$; ****: $p < 0.001$; MAD = mean absolute deviation around the median). **D-E** Throughout selection, ancestral bacterial populations are more diverse than extant ones, as measured by nanopore sequencing of

AS-ANC2lib and AS-AfAdklib timepoints at 42 ºC and subsequent timepoints of 20 ºC selection. Numbers on top identify the total number of variants detected. **F** Sequence logo of low-abundance AS-AfAdklib variants at residues 3-5. Populations in (**D**) and (**E**) are represented as mean ± s.d. of n = 3 replicates and the average number of unique amino acid variants is indicated above each bar. Data for each replicate are provided in Supplementary Tables 2 and 3.

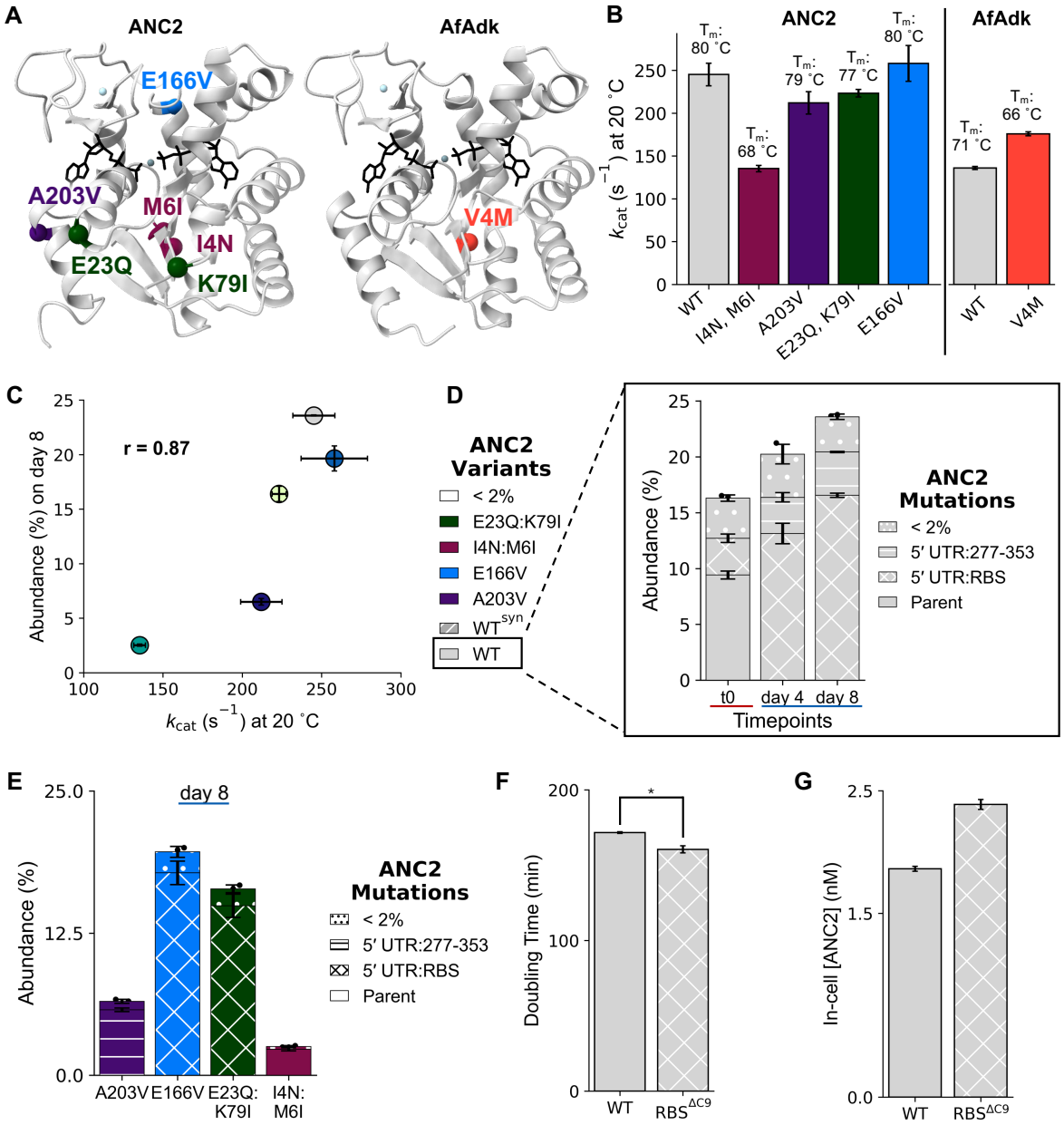

Fig. 3: Selection *in vivo* acts on Adk activity and expression levels. A Mutations for each highly abundant variant after 8 days of selection are plotted onto AlphaFold 3 predictions (as colored spheres) of ANC2 or AfAdk (grey cartoon, depicted as in **Fig. 1E**). **B** k_{cat} of Adk-catalyzed ATP production from 5 mM Mg^{2+}•2ADP by ANC2 and AfAdk variants enriched by selection measured via coupled assay (20 ºC, mean ± s.d. of n ≥ 3 replicates, Supplementary Table 4) and melting temperature (T_m; above bar). **C** Relative abundance of each highly abundant ANC2 variant after 8 days of selection at 20 ºC plotted against its k_{cat} (Pearson r = 0.87) indeed shows enrichment of the fastest variants after selection. **D-E** Mutations in the 5′ UTR (5′ untranslated region) in regions 277-353 and the ribosomal binding site (RBS) are enriched in both the WT (**D**) and 3 of the 4 highly abundant ANC2 variants (**E**). Parent = wild-type vector sequence). Populations are represented as mean ± s.d. of n = 3 replicates. **F** A mutant ANC2 strain harboring the

most common RBS variant, $RBS^{\Delta C9}$ (RBS numbering, see Supplementary Fig. 10H), grows faster at 20 ºC than the ANC2 WT strain (Kolmogorov-Smirnov test: $p = 0.03$, *: $p < 0.05$). **G** In-cell ANC2 concentration was determined in WT and $RBS^{\Delta C9}$ ANC2 strains (grown at 30 ºC) by measuring ATP production in lysate via coupled assay at 20 ºC (mean ± s.d. of $n = 3$; see Methods).

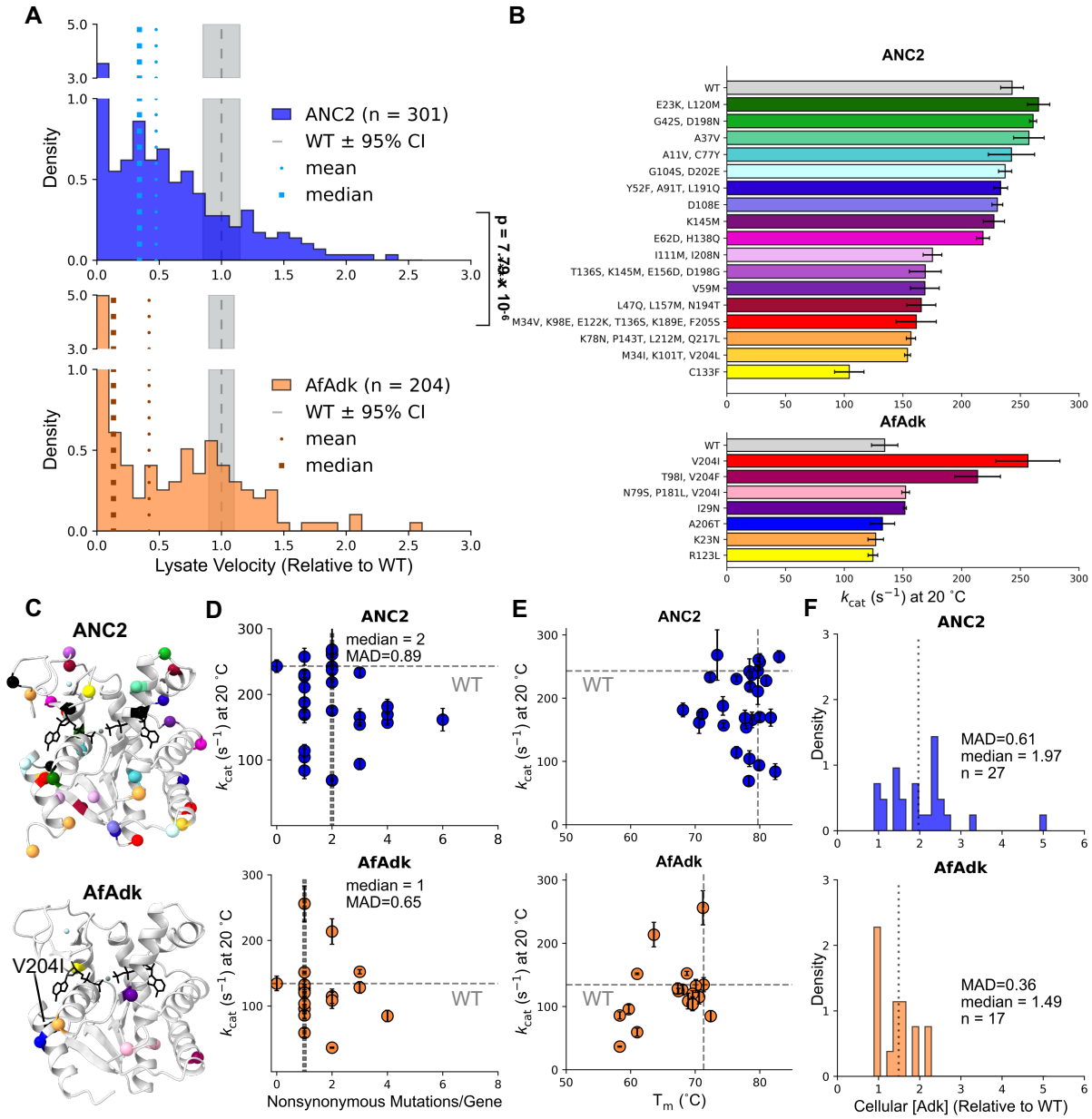

Fig. 4: ANC2 is more robust to mutation than AfAdk in *in vitro* screening. A Histograms of lysate Adk activity (ATP production, coupled assay at 20 ºC) show a significantly different ancestral distribution (Kolmogorov-Smirnov test: $p = 7.79 \times 10^{-6}$), with ANC2 lysates generally being more active than AfAdk lysates (Kolmogorov-Smirnov test: $p = 3.90 \times 10^{-6}$), reflecting an increased mutational robustness in ANC2 over AfAdk ($ANC2_{mean} = 0.48$, $ANC2_{median} = 0.34$, $AfAdk_{mean} = 0.42$, $AfAdk_{median} = 0.13$). **B** Catalytic rates of ATP production by highly active Adk variants measured at 20 ºC, via coupled assay (mean ± s.d. of n ≥ 2 replicates). **C** Mutations for each assayed variant are plotted using the same color as in B onto AlphaFold 3 predictions of ANC2 or AfAdk (grey cartoon, depicted as in **Fig. 1E**, mutations are labeled in Supplementary Fig. 15A). Mutations that appear in more than one variant are colored as black spheres. **D-E** k_{cat} of assayed variants at 20 ºC plotted against number of mutations per gene (**D**) and T_m (**E**) for ANC2 and AfAdk variants. **F** Histogram showing that cellular Adk concentrations of assayed

1109 variants are significantly different (Kolmogorov-Smirnov test: $p = 0.025$), with ANC2
1110 expression levels being generally higher (Kolmogorov-Smirnov test: $p = 0.013$; MAD =
1111 mean absolute deviation around the median, ****: $p < 0.001$).